

Binary nucleation kinetics. V. Φ lines and evaporation rate surfaces

Barbara E. Wyslouzil^{a)}

Department of Chemical Engineering, Worcester Polytechnic Institute, Worcester, Massachusetts 01609-2280

Gerald Wilemski

Department of Physics and Cloud and Aerosol Sciences Laboratory, University of Missouri–Rolla, Rolla, Missouri 65409-0430

(Received 17 August 1998; accepted 7 October 1998)

We explore the quasiuniversal behavior of the function $\Phi(i,j,t) = f(i,j,t)/N(i,j,t)$ in binary nucleation, where $f(i,j,t)$ and $N(i,j,t)$ are the nonequilibrium and equilibrium cluster concentrations, respectively. The simple, regular patterns that are formed by this function during both the transient period and at steady state suggest that the contour lines of constant Φ form one half of a natural curvilinear coordinate system that underlies the binary nucleation process. In this paper we present the Φ -line patterns for binary systems that display a wide range of liquid phase nonideality. Quantitative comparisons between analytical expressions for the angle that $\nabla\Phi$ makes with the component A axis and for the spacing of the Φ contour lines give good agreement with the values derived from the numerical solution of the binary kinetics equations. The insensitivity of the Φ -line patterns to changes in the gas phase activities of the nucleating species can be better understood by writing the binary kinetics equations with the evaporation rate coefficients as the “diffusion coefficients.” In this form it is easy to see that the equations only depend weakly on the actual gas phase compositions. © 1999 American Institute of Physics. [S0021-9606(99)51402-5]

I. INTRODUCTION

In our recent work on binary nucleation kinetics, we explored issues of self-consistency in the equilibrium cluster distribution¹ and solved the binary kinetics equations to better understand both steady state² and transient³ binary nucleation. By examining binary systems that exhibited a wide range of liquid solution behavior, and by systematically varying the binary system parameters, including impingement rates, equilibrium vapor pressures, and vapor phase activities, we gained an appreciation for the dynamic behavior of the free energy surfaces, the steady state flux patterns and the transient behavior of the cluster fluxes and cluster concentrations.

One unexpected result, discussed briefly in part III of this series,³ was that the ratio of the nonequilibrium cluster concentration $f(i,j,t)$ to the equilibrium cluster concentration $N(i,j,t)$, $\Phi(i,j,t) = f(i,j,t)/N(i,j,t)$, exhibits a quasiuniversal behavior for each binary system. For widely varying gas phase activities and monomer impingement rates, the pattern formed by contours of constant Φ , which we call Φ lines, appears remarkably unchanged. The qualitative appearance of the Φ lines depends primarily on the thermodynamic properties of the liquid mixture, particularly on the relative sizes of the evaporation rate coefficients. In this paper we present a more complete examination of the phenomenon, explain how it arises from the invariance of the cluster evaporation rate coefficients, and discuss how the Φ lines form a set of natural coordinates underlying the binary nucleation process. In Sec. II of this paper we briefly summarize

the kinetics equations that we solved. Steady state and transient results are presented and discussed in Secs. III and IV, respectively. Section V summarizes the work.

II. COMPUTATIONAL METHODOLOGY

As in our previous work, the kinetics equations describing binary nucleation^{2,3} were solved assuming that clusters grow and decay only by adding or losing monomers. The time rate of change of the number density of clusters containing i molecules of species A and j molecules of species B is given by

$$\frac{df(i,j,t)}{dt} = J_A(i-1,j,t) - J_A(i,j,t) + J_B(i,j-1,t) - J_B(i,j,t), \quad (1)$$

where the fluxes J_A and J_B between adjacent cluster sizes are given by

$$J_A(i,j,t) = \Gamma_A(i,j)N_A f(i,j,t) - E_A(i+1,j)f(i+1,j,t), \quad (2)$$

and

$$J_B(i,j,t) = \Gamma_B(i,j)N_B f(i,j,t) - E_B(i,j+1)f(i,j+1,t). \quad (3)$$

The rate coefficient for adding a monomer of type ν to a cluster with composition (i,j) is $\Gamma_\nu(i,j)$, while $E_\nu(i,j)$ is the rate coefficient for removing a monomer of species ν from a cluster with composition (i,j) . The monomer concentrations are defined as $N_A = f(1,0,t)$ and $N_B = f(0,1,t)$. The collision frequency between two particles of unequal mass, taken from the kinetic theory of gases, is used for the for-

^{a)}Electronic mail: barbaraw@wpi.edu

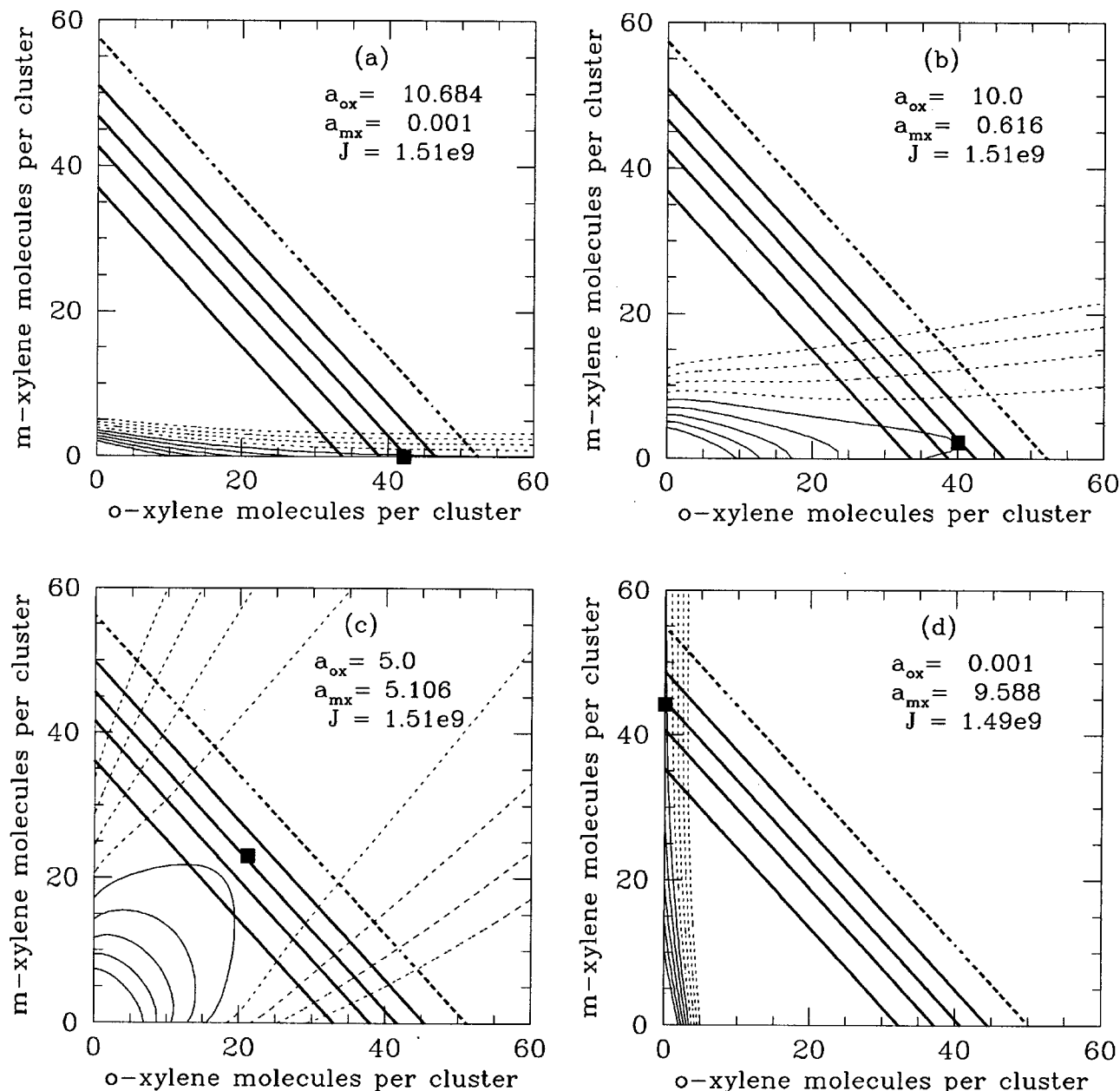


FIG. 1. Lines of constant Φ (heavy lines) are superimposed on contour lines of constant cluster concentration (light solid and dashed lines) for the o-xylene-m-xylene system at four different sets of vapor phase activities. The analytical saddle points are marked by solid squares. The $\Phi=0.1$ contour is the heavy dashed line and the Φ contour lines increase in steps of 0.2. For the cluster concentrations, the contour line closest to the origin corresponds to 10^8 cm^{-3} . The cluster concentration contour lines then decrease by factors of 100, with the last solid contour line corresponding to a cluster concentration of 1 cm^{-3} . The dashed contour lines correspond to cluster concentrations in the range 10^{-2} – 10^{-8} cm^{-3} .

ward rate coefficients assuming a unit mass accommodation coefficient for each species. The principle of detailed balance, together with the forward rate coefficients and the equilibrium cluster size distribution, is used to define the reverse rate coefficients. The rate coefficients asymptotically approach the expressions used in conventional binary nucleation theory for large i and j , while the rate coefficients for small i and j differ from the conventional ones because of the self-consistency corrections that we introduced into the equilibrium distribution. Explicit expressions for the rate coefficients and the equilibrium distribution used are available in parts I and II of this series,^{1,2} with one significant difference. We now use the following expression⁴ for the reversible work of formation of the cluster $W(i, j)$:

$$\frac{W(i, j)}{kT} = \ln \left(\frac{i!j!}{(i+j)!} \right) - i \ln \left(\frac{a_A}{\gamma_A} \right) - j \ln \left(\frac{a_B}{\gamma_B} \right) + \frac{4\pi r^2 \sigma}{kT}, \quad (4)$$

where a_v is the vapor phase activity of a nucleating species, γ_v is a liquid phase activity coefficient, r is the cluster radius assuming a spherical cluster, σ is the bulk surface tension at the overall composition of the cluster, k is the Boltzmann constant, and T is the temperature. For very large values of i and j this expression approaches⁵ the conventional expression for $W(i, j)$, but for small clusters, Eq. (4) ensures that the entropy of mixing term is not overestimated.⁶ Introducing this change in the definition of $W(i, j)$ means that the nucleation rates calculated here differ from those presented in our

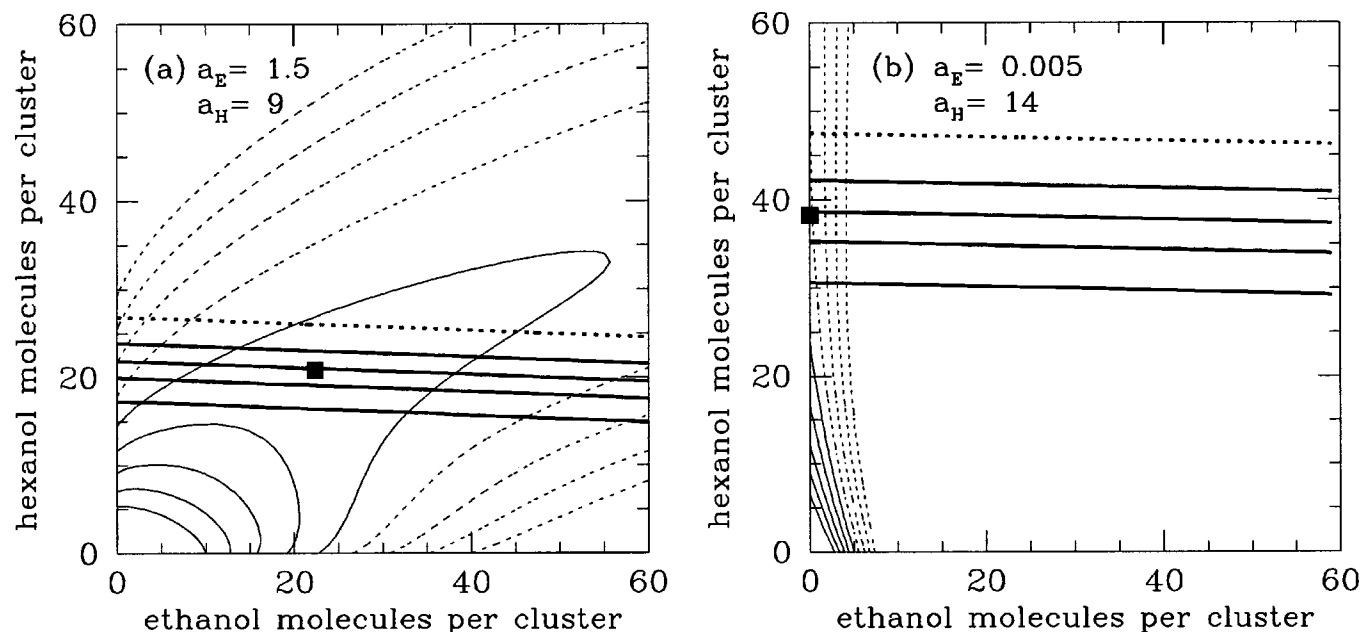


FIG. 2. Lines of constant Φ (heavy lines) are superimposed on contour lines of constant cluster concentration (light solid and dashed lines) for the ethanol–hexanol system at two different sets of vapor phase activities. The contour lines are scaled as in Fig. 1, and the analytical saddle points are marked by solid squares.

previous work although the limits of unary nucleation remain the same. Explicit expressions for the Kelvin equations stemming from Eq. (4) are given in the Appendix. The initial conditions, boundary conditions and related computational details are the same as in our previous work.^{2,3} The physical properties of the binary systems are available in Ref. 2. As in our previous work,² the numerical nucleation rates generally agree with the analytical rates, calculated using the Stauffer⁷ rate expression, to within 10% as long as the major nucleation flux passes through the saddle point.

III. STEADY STATE RESULTS

A. Φ -line patterns

We begin by presenting several figures that illustrate the quasiuniversal behavior that is the underlying theme of this paper. The point is particularly well illustrated by the Φ lines in the highly ideal *o*-xylene–*m*-xylene system, under conditions for which the final nucleation rate varies by less than 2%. In Fig. 1 the dynamic response of the steady state cluster concentrations to changes in the vapor phase activities and impingement rates contrasts starkly with the invariance of the Φ lines. For the chosen vapor phase activities, the nucleation process changes from one in which most of the new droplets are formed by unary nucleation of *o*-xylene to one in which unary nucleation of *m*-xylene is the dominant pathway, and the monomer impingement rate ratios of *o*-xylene to *m*-xylene vary from 8.5×10^3 to 8.3×10^{-5} . As in unary nucleation, the steady state cluster concentration at the saddle point equals one half the equilibrium concentration. We can characterize the orientation of the Φ lines by the angle ω between $\nabla\Phi$ at the saddle point and the component *A* axis.⁸ In this nearly degenerate system ω is close to 45° because the values of all the physical properties of *o*-xylene

are close to those of *m*-xylene. For example, the equilibrium vapor pressures of the two species differ by only 26%, 0.665 and 0.839 kPa, respectively, at the simulation temperature of 293.5 K.

For a truly degenerate binary system, i.e., when the two species are indistinguishable except for an arbitrary label, the symmetry of the problem forces $\omega = 45^\circ$ exactly. This is easily seen by simply relabeling the two species. Alternatively, an analytical derivation of this result is given in the Appendix. If one solves the binary kinetics equations numerically using the *conventional* expression for W , the Φ lines bend near the pure component axes even for the ideal degenerate system. This physical inconsistency is a direct consequence of an entropy of mixing term that is too large.⁶ The symmetry of the degenerate system also dictates that the position of the Φ lines cannot vary at a constant nucleation rate. Looking more closely at Fig. 1, we see that in the *o*-xylene–*m*-xylene system the positions of the Φ lines do shift slightly as the gas phase activities are varied. The changes reflect the fact that the physical properties of *m*-xylene (vapor pressure, surface tension and molecular volume) are not identical to those of *o*-xylene, and the critical cluster for pure *o*-xylene nucleation contains fewer molecules than the critical cluster for pure *m*-xylene nucleation at the same nucleation rate. Figures 1(a) and 1(d) represent the limits of the nucleation process in this binary system, and we expect a smooth variation between these extremes for intermediate values of the vapor phase activities.

Figure 2 shows the Φ -line signatures for a second binary system, ethanol–hexanol, whose components form an ideal liquid mixture but have equilibrium vapor pressures that differ significantly. At the simulation temperature, the equilibrium vapor pressure of ethanol is approximately 230 times higher than that of hexanol. The Φ lines are nearly parallel to

the ethanol axis because of the tendency of clusters to rapidly “equilibrate” with respect to ethanol, regardless of the actual gas species impingement rates. In Fig. 2(b), for example, the gas phase activity ratio (hexanol/ethanol) is 2800, the impingement rate ratio is approximately 8.3, and the gas phase composition ratio (N_H/N_E) is 12.4. All of these factors would seem to heavily favor rapid equilibration of the concentrations of hexanol-rich clusters, yet the concentrations of ethanol-rich clusters still equilibrate more rapidly. As discussed below, this behavior is closely related to the tendency of the evaporation rate of ethanol E_E to exceed that of hexanol E_H for most cluster compositions. In contrast to the behavior of the Φ lines, under these extreme conditions the fluxes develop most rapidly along the hexanol axis, closely following the transient evolution of the absolute cluster concentrations.

In both Figs. 1 and 2, the Φ lines appear to be straight. To test whether this is true we measured the slope (in degrees) along the $\Phi=0.5$ contour using the numerical output from our contouring program. For the o-xylene–m-xylene system under the conditions in Fig. 1(c) the slope is 42.4° , and is constant to four significant figures. For the ethanol–hexanol system under the conditions in Fig. 2(a) the slope is 88.0° when $i=3$, when $i=i^*=22.4$ the slope is 87.8° , and when $i=60$ the slope is 87.6° . At the saddle point (i^*,j^*) the measured slope should be equal to ω . In recent papers, Wilemski⁸ and Li, Nishioka and Maksimov^{9–11} independently showed that ω is related to Stauffer’s flux angle ϕ by the simple relationship:

$$r_S \tan \omega = \tan \phi, \quad (5)$$

and ϕ is given by⁷

$$\tan \phi = s + \sqrt{s^2 + r_S}, \quad (6)$$

with the ratio of impingement rates defined as

$$r_S = \frac{\Gamma_B(i^*,j^*)N_B}{\Gamma_A(i^*,j^*)N_A}, \quad (7)$$

and

$$2s = (r_S W_{BB} - W_{AA})/W_{AB}. \quad (8)$$

We denote the three second derivatives of $W(i,j)$ at the saddle point as W_{AA} , W_{AB} , and W_{BB} . The analytical predictions for ω at the saddle point calculated using Eqs. (5)–(8) are 42.4° for o-xylene–m-xylene and 87.9° for ethanol–hexanol. In both cases the agreement is excellent.

To examine the effect of liquid phase nonideality, Figs. 3(a)–3(d) show the Φ -line plots for a negatively deviating system dichloromethane–tetrahydrofuran (DCM–THF) and two positively deviating systems, PD1 and PD2. As in our previous work, the PD1 and PD2 systems have all of the physical properties of the o-xylene–m-xylene and ethanol–hexanol systems, respectively, with the exception that the excess Gibbs free energy of mixing is given by the simple regular solution expression:

$$g^E = A x_A x_B, \quad (9)$$

where x_ν is the mole fraction of species ν in the cluster and $A/(kT) = 2$ at the simulation temperature. This choice of A

places both systems at their upper critical solution temperatures and results in a broad free energy surface. Liquid mixtures that deviate negatively from ideality have Φ lines with inward curvature while positively deviating systems have Φ lines with outward curvature. The PD1 system exhibits the same symmetry inherent in the o-xylene–m-xylene system, while the Φ lines for the PD2 system parallel the ethanol axis reminiscent of the behavior in the underlying ethanol–hexanol system. One interesting feature of the PD2 system is that for certain vapor phase activities the major steady state particle flux avoids the saddle point and nucleation occurs via ridge crossing.² When nucleation occurs by ridge crossing, the value of Φ at the saddle point is far below 0.5 because the cluster concentrations in the vicinity of the saddle point are suppressed. In essence, the clusters that would have grown to form saddle point clusters are swept over the ridge prematurely. Figure 3(d) is an example of such a case and yet the characteristic Φ -line pattern has hardly changed from that of Fig. 3(c). We also note that in Fig. 3(c) the saddle point appears to lie at a slightly higher value of Φ than 0.5. Here, the discrepancy between the analytical nucleation rate, $J = 1.73 \times 10^6$, and the numerical rate, $J = 2.98 \times 10^6$, is already much larger than the $\sim 10\%$ agreement typically observed² for systems with saddle regions that are less flat. In this case, saddle point nucleation is still the dominant particle formation pathway, but the total flux passing through the broadened saddle region is now underestimated by the usual parabolic approximation for the flux on either side of the saddle point.

Since the Φ -line pattern is not affected by the nucleation pathway, we can understand the curvature in the Φ lines illustrated in Fig. 3 by considering only the usual case of saddle point nucleation and conducting the following thought experiment. First consider the behavior for clusters forming ideal liquid mixtures. For given vapor phase activities, the critical cluster has a certain size and composition, and the Φ lines are straight. If the activities and other physical properties are now held fixed but the liquid mixture is now imagined to deviate negatively from ideality, the supersaturation of each component will increase, and the critical cluster size will decrease.¹² Since the critical cluster still lies on the $\Phi = 0.5$ line and since this line’s intercepts with the i and j axes are fixed by the constancy of physical properties and conditions, the $\Phi = 0.5$ line is now “stretched” toward the origin, i.e., bowed inward relative to ideal behavior. Obviously, a corresponding argument can be constructed to explain the outward curvature present for positively deviating liquid mixtures.

In Figs. 1 and 2, the angle ω is not a strong function of gas phase composition or the saddle point location. If we imagine a series of similar plots for the positively or negatively deviating systems, it is clear that although the Φ -line pattern does not change much as the gas phase compositions vary, the angle ω at the saddle point will change systematically as the saddle point moves from being close to the component A axis to being close to the component B axis. We are now in a position to directly test this relationship by comparing the numerically measured slope at the saddle point (in

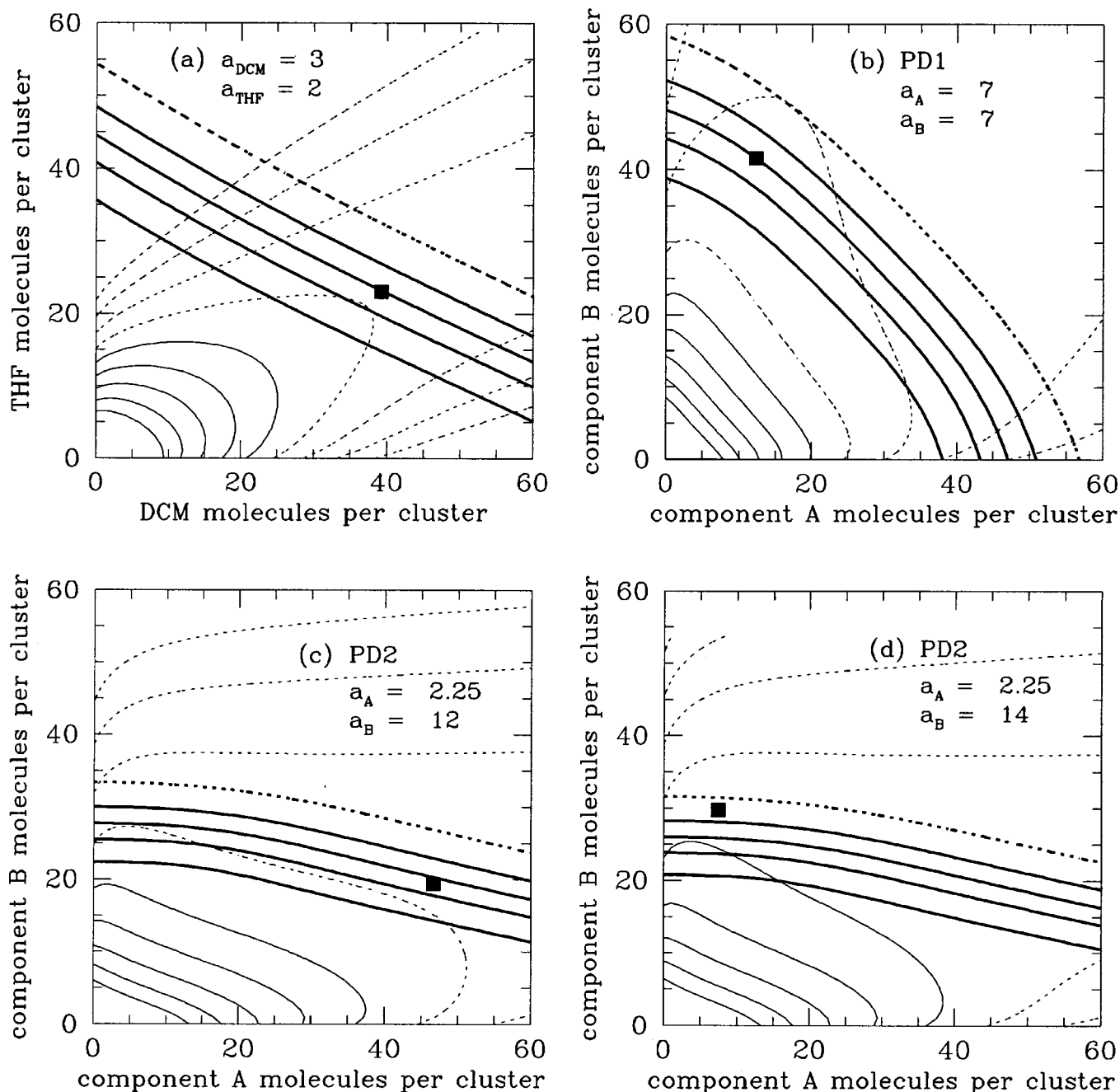


FIG. 3. Lines of constant Φ (heavy lines) are superimposed on contour lines of constant cluster composition (light solid and dashed lines) for three additional binary systems. The contour lines are scaled as in Fig. 1, and the analytical saddle points are marked by solid squares. (a) In the dichloromethane-tetrahydrofuran system the Φ lines bow in toward the origin. (b) In the PD1 system the Φ lines bow away from the origin, and the pattern exhibits much of the symmetry inherent in the underlying *o*-xylene-*m*-xylene system. (c) In the PD2 system the Φ lines bow away from the origin, and the pattern exhibits an asymmetry similar to that in the underlying ethanol-hexanol system. Saddle point nucleation is still the major pathway. (d) In this second example for the PD2 system, most of the new phase forms via a ridge crossing pathway, and saddle point nucleation is much less important.

degrees) with the analytically predicted value for ω as the vapor phase activities and r_S are systematically varied. Figure 4 illustrates that there is excellent agreement between these two quantities. In contrast to the behavior of ω , the angle ϕ always has essentially the same dependence on r_S for all binary systems. As $r_S \rightarrow 0$, $\phi \rightarrow 0^\circ$, and unary nucleation of component A is the nucleation pathway. As $r_S \rightarrow \infty$, $\phi \rightarrow 90^\circ$, and unary nucleation of component B is the only pathway.

The regularity and simplicity of the Φ -line patterns for

the wide range of systems that we have examined, suggests that a curvilinear coordinate system⁸⁻¹⁰ with one axis parallel to the Φ lines and the other axis (ζ) orthogonal to them is ideally suited for reducing the variation of Φ to an effective one-dimensional problem in the ζ coordinate. In the vicinity of the saddle point the curvilinear system is effectively Cartesian and is straightforward to implement.⁸ This approach was recently used to rederive Trinkaus's¹³ analytical solution for Φ in the vicinity of the saddle point.⁸ In terms of ζ , the solution is given by

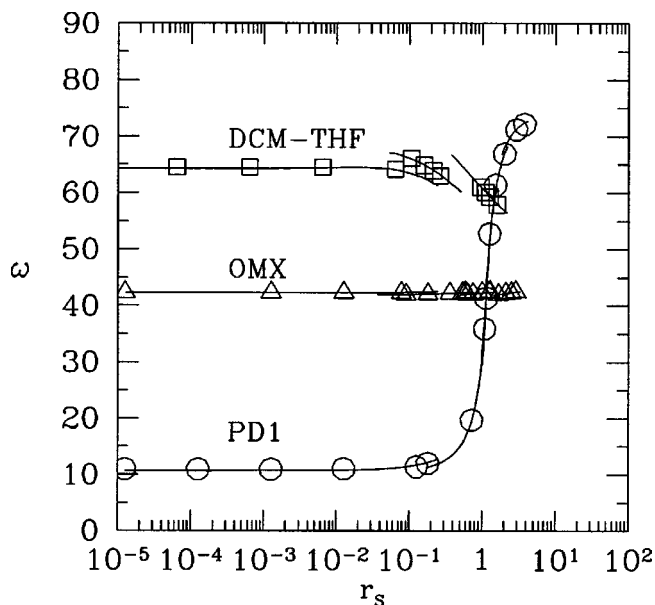


FIG. 4. The values of ω measured at the saddle point (symbols) are in excellent agreement with those predicted by Eqs. (5)–(8) (solid lines) over the entire range of the parameter r_s . As shown by the DCM-THF system, the angle ω depends on the actual vapor phase activities and not just the value of r_s .

$$\Phi(\zeta) = \frac{1}{2} \operatorname{erfc}(\sqrt{\Lambda/2}\zeta), \quad (10)$$

where

$$\zeta = (i - i^*) \cos \omega + (j - j^*) \sin \omega, \quad (11)$$

$$\Lambda = L / (R_A^* \cos^2 \omega + R_B^* \sin^2 \omega), \quad (12)$$

$$L = -[R_A^* W_{AA} \cos^2 \omega + (R_A^* + R_B^*) W_{AB} \cos \omega \sin \omega + R_B^* W_{BB} \sin^2 \omega] / (kT), \quad (13)$$

and

$$R_\nu^* = \Gamma_\nu(i^*, j^*) N_\nu. \quad (14)$$

$$\begin{aligned} \frac{\partial \Phi}{\partial t} = & \Gamma_A(i-1, j) N_A N(i-1, j) / N(i, j) [\Phi(i-1, j, t) - \Phi(i, j, t)] + \Gamma_B(i, j-1) N_B N(i, j-1) / N(i, j) [\Phi(i, j-1, t) - \Phi(i, j, t)] \\ & - \Gamma_A(i, j) N_A [\Phi(i, j, t) - \Phi(i+1, j, t)] - \Gamma_B(i, j) N_B [\Phi(i, j, t) - \Phi(i, j+1, t)], \end{aligned} \quad (15)$$

and

$$\begin{aligned} \frac{\partial \Phi}{\partial t} = & E_A(i, j) [\Phi(i-1, j, t) - \Phi(i, j, t)] + E_B(i, j) [\Phi(i, j-1, t) - \Phi(i, j, t)] - E_A(i+1, j) N(i+1, j) / N(i, j) \\ & \times [\Phi(i, j, t) - \Phi(i+1, j, t)] - E_B(i, j+1) N(i, j+1) / N(i, j) [\Phi(i, j, t) - \Phi(i, j+1, t)]. \end{aligned} \quad (16)$$

The advantage of writing the equations in the latter form is that E_A and E_B are now the “diffusion coefficients” rather than $\Gamma_A N_A$ and $\Gamma_B N_B$. Thus Eq. (16) shows directly how a disparity between E_A and E_B can lead to a rapid increase of Φ in one direction with much slower progress in the other. In

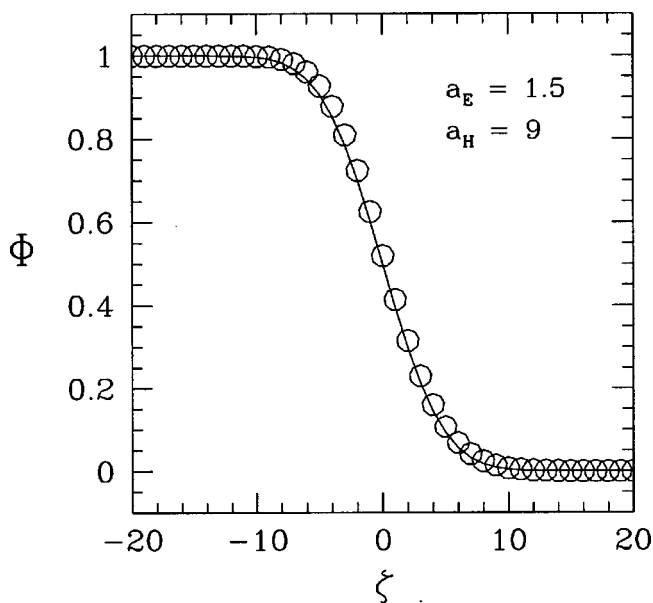


FIG. 5. The circles are the numerical values of $\Phi(\zeta)$ for the conditions in Fig. 2(a). The solid line was calculated using Eq. (10).

With this result we can now test our ability to predict the spacing of the Φ lines. Figure 5 compares the analytically predicted variation of Φ with the numerical values for the conditions in Fig. 2(a). Clearly the analytical result provides a good fit to the numerical values over a wide range of ζ , and thus it is now possible to calculate actual cluster concentrations in the vicinity of the saddle point without recourse to the full numerical solution.

B. Evaporation rate surfaces

As briefly discussed in our previous work³ the invariance of the Φ lines can be better appreciated by transforming Eq. (1) into two equivalent equations for the time evolution of Φ . Applying the detailed balance relations lets us write the equations in terms of either the forward rate coefficients or the evaporation rate coefficients. The results are

the usual ideal gas approximation, the evaporation rate coefficients are independent of the gas phase activities and the total pressure. Thus changes in the vapor phase activities only affect the time and composition dependence of Φ through the ratios $N(i+1, j) / N(i, j)$ and $N(i, j+1) / N(i, j)$.

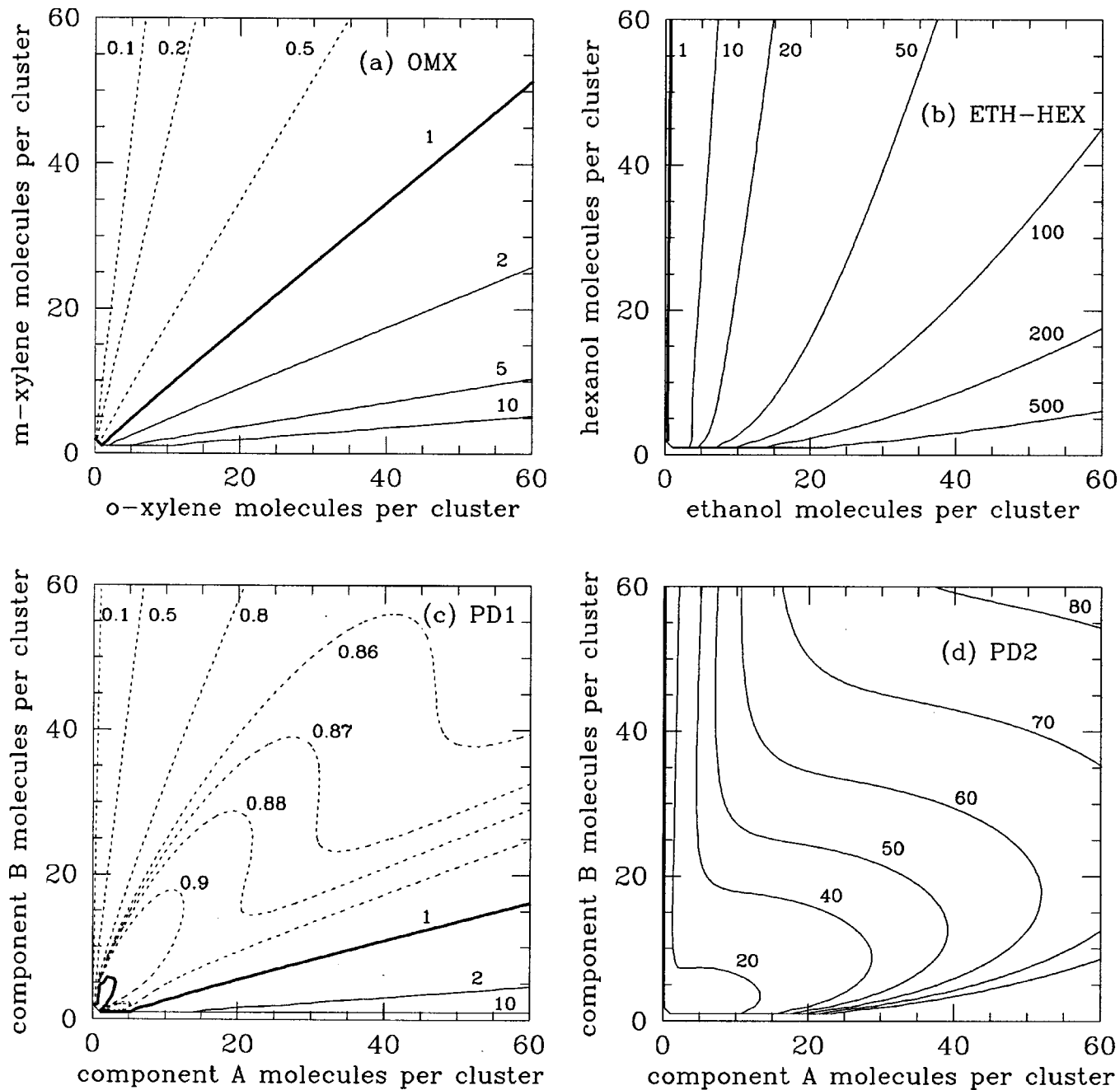


FIG. 6. Contours of constant E_A/E_B are shown for the two ideal and the two positively deviating systems. The looped appearance of the evaporation rate surfaces in the positively deviating systems is due to the parabolic mean field approximation inherent in the nonideal free energy of mixing term, Eq. (9).

Near the saddle point these ratios are close to 1 and the dependence on the vapor composition is correspondingly very weak. Thus the transient and steady state contour plots of Φ have a characteristic "signature" that depends predominantly on the relative sizes of E_A and E_B for each system.

In order to examine the relative behavior of the evaporation rate coefficients as a function of cluster composition and size, we have chosen to examine how the ratio E_A/E_B varies. Figures 6(a)–6(d) show the contour plots of the ratios E_A/E_B for four of the systems discussed so far. In all cases, the limits of the ratios are $E_A/E_B \rightarrow \infty$ along the pure component A axis while $E_A/E_B \rightarrow 0$ along the pure component B

axis. In the ideal degenerate case, the contour lines of E_A/E_B and E_B/E_A are completely symmetric about the $E_A/E_B = 1$ line which would itself make a 45° angle with the component A axis. The high degree of symmetry in the physical properties of o-xylene and m-xylene results in a plot that approaches ideal, degenerate system behavior, and the rate of cluster equilibration is largely independent of cluster composition. In contrast, the $E_A/E_B = 1$ line in the ethanol–hexanol system lies very close to the pure hexanol axis. Thus for all mixed clusters included in the simulation, the evaporation rate coefficient for ethanol is higher than the evaporation rate coefficient for hexanol. This inequality is responsible for the rapid equilibration of the cluster concentrations in the etha-

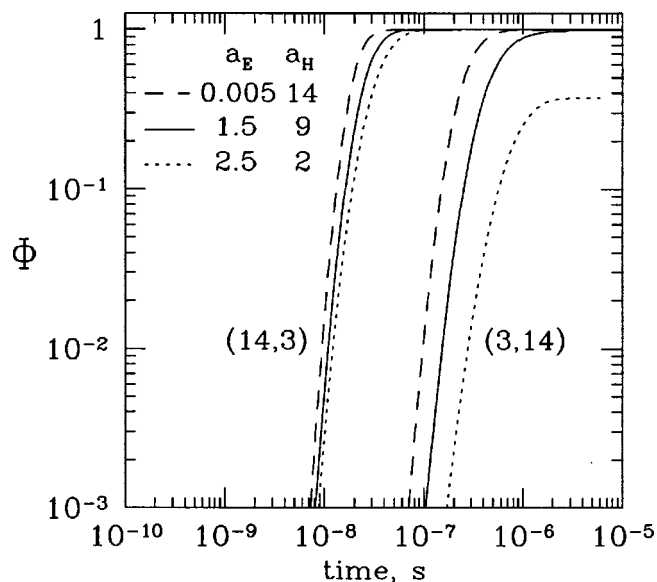


FIG. 7. The time evolution of Φ for two cluster compositions in the ethanol-hexanol system. The cluster composition is indicated by the notation (i, j) . For subcritical clusters, $\Phi(t)$ depends primarily on the cluster composition and is remarkably insensitive to the actual gas phase activities. When $a_E = 2.5$, clusters containing 14 molecules of hexanol are supercritical, and their steady state value of $\Phi \approx 0.4$.

nol direction. The curvature in the ethanol-hexanol contours at small (i, j) is due to the Kelvin term, $\exp[\Omega(i, j) - \Omega(i-1, j)]$ where $\Omega(i, j) = 4\pi r^2(i, j)\sigma(i, j)/(kT)$. This term amplifies differences in the surface tensions and molecular volumes of ethanol and hexanol. Although not shown here, the evaporation rate surfaces for the negatively deviating systems are qualitatively the same as the ideal systems. More interesting is the behavior observed in the positively deviating systems. Both the PD1 and PD2 systems shown in Fig. 6 display contours that bend back upon themselves. This consequence of mean-field nonideal solution thermodynamics is a harbinger of the more complex evaporation rate surfaces that exist for phase separating systems. The behavior in Fig. 6(d) is particularly striking. Because PD2 is a system for which ridge crossing occurs, evaporation rate surfaces that look like Fig. 6(d) are indicative that ridge crossing behavior is possible. Because of their intrinsic interest it would be useful to have convenient ways to identify potentially ridge crossing systems. It is clearly easier to look at a single evaporation rate surface than to examine many free energy surfaces, whose shape strongly depends on the gas phase activities, until a characteristic ridge is found. An alternative method using a generalized kinetic potential has recently been suggested by Li *et al.*¹⁰

IV. TRANSIENT RESULTS

Another consequence of the quasiuniversal behavior of the Φ lines is that subcritical clusters, and even small supercritical clusters, reach their steady state concentrations at roughly the same time independent of the vapor phase activities. This phenomenon is illustrated in Fig. 7 by tracking the transient concentrations of two types of clusters in the ethanol-hexanol system at three different vapor phase activities. The two types of clusters have the same total numbers

of molecules but very different overall compositions. In all cases the hexanol-rich cluster concentrations always take about ten times longer to reach their steady state values than do the ethanol-rich cluster concentrations. The fact that the Φ values of both cluster types reach their steady state values faster as a_H increases demonstrates, in a different way from Fig. 2, that under most conditions equilibration with hexanol is the rate limiting process. We note again that the absolute values of the cluster concentrations vary by many orders of magnitude as the vapor phase activities change, but the approach to steady state remains remarkably consistent.

V. SUMMARY AND CONCLUSIONS

In this paper we have explored the qualitative behavior of the Φ -line patterns as a function of physical parameters of the binary nucleating components. We have demonstrated that we can quantitatively predict the angle made by the Φ lines at the saddle point. We have shown how the remarkable consistency of the patterns can be understood by thinking of the nucleation process as diffusion in composition space with an anisotropic diffusivity determined by the evaporation rate coefficients. At a given temperature, each binary system has a unique evaporation rate surface that largely determines the characteristic Φ -line pattern. These plots can help us spot systems for which ridge crossing might occur. The transient evolution of Φ for both subcritical and small supercritical clusters also shows quasiuniversal behavior.

ACKNOWLEDGMENTS

This work was supported by the National Science Foundation, Division of Chemistry under Grant No. CHE-9502604 (BEW) and by the U.S. Department of Energy, Office of Basic Energy Sciences, Division of Geosciences and Engineering (GW).

APPENDIX

In this Appendix we find analytical expressions for $\tan \omega$ for ideal systems. For the reversible work of cluster formation given in Eq. (4), the two Kelvin equations that determine the location of the saddle point are given by

$$0 = \Psi(i+1) - \Psi(n+1) - \ln x_A - \ln \frac{a_A}{x_A \gamma_A} + \frac{2\sigma v_A}{kTr} - \frac{3v}{kT} \frac{x_B}{r} \frac{d\sigma}{dx_B}, \quad (\text{A1})$$

and

$$0 = \Psi(j+1) - \Psi(n+1) - \ln x_B - \ln \frac{a_B}{x_B \gamma_B} + \frac{2\sigma v_B}{kTr} + \frac{3v}{kT} \frac{x_A}{r} \frac{d\sigma}{dx_B}, \quad (\text{A2})$$

where $n = i + j$, v_v is the partial molecular volume of species v , v is the mean molecular volume, and the other symbols have been defined in the main body of the paper. The psi function Ψ is defined by Gradshteyn and Ryzhik¹⁴ as

$$\Psi(i+1) = \frac{d \ln i!}{di} = -\gamma_E + \sum_{p=0}^{\infty} \left(\frac{1}{p+1} - \frac{1}{i+p+1} \right), \tag{A3}$$

where $\gamma_E = 0.5772 \dots$ is the Euler–Mascheroni constant.

Although they are thermodynamically incorrect,^{15,16} the surface tension derivatives appear in Eqs. (A1) and (A2) because the physics needed to eliminate them is missing in our well mixed droplet model. Because of this, the derivatives are implicit in all of our numerical solutions and thus they must be retained in the Kelvin equations to permit a direct comparison of the numerical and analytical nucleation rates. In general, these nonlinear equations must be solved simultaneously to obtain the size and composition of the critical nucleus. We have done this for many different cases and found that the numerical solutions generally differ only slightly from those of the conventional approach. Usually i and j differ by less than 0.5 each from the values calculated by solving the conventional equations,

$$0 = -\ln \frac{a_A}{x_A \gamma_A} + \frac{2\sigma v_A}{kTr} - \frac{3v}{kT} \frac{x_B}{r} \frac{d\sigma}{dx_B}, \tag{A4}$$

and

$$0 = -\ln \frac{a_B}{x_B \gamma_B} + \frac{2\sigma v_B}{kTr} + \frac{3v}{kT} \frac{x_A}{r} \frac{d\sigma}{dx_B}. \tag{A5}$$

We will therefore continue the development using Eqs. (A4) and (A5) with little loss of accuracy. Furthermore, to make the presentation more transparent, we now set the surface tension derivative to zero and specialize to ideal systems by putting $\gamma_A = \gamma_B = 1$.

Based on the conventional definition of W , the second derivatives for an ideal system¹⁷ are given by

$$W_{AA} = j^* kT / (i^* n^*) - \alpha v_A^2 / (n^* v)^{4/3}, \tag{A6}$$

$$W_{BB} = i^* kT / (j^* n^*) - \alpha v_B^2 / (n^* v)^{4/3}, \tag{A7}$$

and

$$W_{AB} = -kT/n^* - \alpha v_A v_B / (n^* v)^{4/3}, \tag{A8}$$

where

$$\alpha = \frac{8\pi\sigma(3/4\pi)^{2/3}}{9}. \tag{A9}$$

In order to evaluate Eq. (5) for $\tan \omega$ we first need to evaluate the parameter s defined by Eq. (8). Using Eqs. (A6)–(A8) it is easy to show that

$$2s = \left[\frac{j^*}{i^*} - \frac{r_S i^*}{j^*} + \frac{2}{3} \frac{w_{cl}^*}{n^*} \left(\frac{r_S v_B^2 - v_A^2}{v^2} \right) \right] / \left(1 + \frac{2}{3} \frac{w_{cl}^*}{n^*} \frac{v_A v_B}{v^2} \right), \tag{A10}$$

where

$$w_{cl}^* = \frac{4\pi}{3} \frac{r^2 \sigma}{kT} = \frac{1}{2} n^* \ln \left(\frac{a_A}{x_A} \right)^{x_A} \left(\frac{a_B}{x_B} \right)^{x_B}. \tag{A11}$$

For an ideal degenerate system, $v_A = v_B = v$, $r_S = y_B/y_A$, where $y_\nu = N_\nu / (N_A + N_B)$, and the solution to the two Kelvin equations, (A4) and (A5), is $x_A^* = y_A$. With these simplifications it is easy to show that Eq. (A10) reduces to

$$2s = (j^* - i^*) / i^*, \tag{A12}$$

and from Eqs. (5) and (6) it follows that

$$\tan \omega = 1. \tag{A13}$$

Thus for an ideal degenerate system, ω is always 45° and independent of the gas phase composition.

A second special case is the limit in which one component vanishes from the mother phase. Because every system approaches ideal behavior for small enough values of a_A or a_B , the following results are valid for nonideal systems as well. As $a_B \rightarrow 0$ at a fixed value of a_A , the approximate solution of the Kelvin equations is

$$x_B^* \approx a_B / a_A^{(v_B/v_A)}, \tag{A14}$$

and $x_B^* \rightarrow 0$. Aside from some i and j dependent factors of order unity, r_S can be expressed as

$$r_S = \frac{a_B}{a_A} \frac{N_B^\infty}{N_A^\infty} \left(\frac{M_A}{M_B} \right)^{1/2}, \tag{A15}$$

where N_ν^∞ is the equilibrium vapor number density of species ν and M_ν is its molecular weight. Thus, as $a_B \rightarrow 0$, r_S also approaches zero. It follows from Eqs. (A10), (A14), and (A15) that in this limit

$$2s = - \left[\frac{N_B^\infty}{N_A^\infty} \left(\frac{M_A}{M_B} \right)^{1/2} a_A^{v_B/v_A - 1} + \frac{2w^*}{3n^*} \left(\frac{v_A}{v} \right)^2 \right] / \left[1 + \frac{2w^*}{3n^*} \left(\frac{v_A v_B}{v^2} \right)^2 \right], \tag{A16}$$

which is a well defined quantity. Since $s < 0$, it also follows from Eqs. (5) and (6) that in this limit

$$\tan \omega = 1 / (2|s|). \tag{A17}$$

In the opposite case, when $a_A \rightarrow 0$ both r_S and s diverge, i.e., $r_S \rightarrow \infty$ and $s \rightarrow \infty$, but $x_A^* \rightarrow 0$, and the quantity $2s/r_S$ is well defined and is given by

$$\frac{2s}{r_S} = \left[\frac{N_A^\infty}{N_B^\infty} \left(\frac{M_B}{M_A} \right)^{1/2} a_B^{v_A/v_B - 1} + \frac{2w^*}{3n^*} \left(\frac{v_B}{v} \right)^2 \right] / \left[1 + \frac{2w^*}{3n^*} \left(\frac{v_A v_B}{v^2} \right)^2 \right]. \tag{A18}$$

In this limit

$$\tan \omega = \frac{2s}{r_S}. \tag{A19}$$

An amusing consequence of either Eq. (A17) or Eq. (A19) is that, just like the lingering grin of the Cheshire cat,¹⁸ the Φ -line pattern of the underlying binary system persists in the limit of unary nucleation.

¹G. Wilemski and B. E. Wyslouzil, J. Chem. Phys. **103**, 1127 (1995).

²B. E. Wyslouzil and G. Wilemski, J. Chem. Phys. **103**, 1137 (1995).

- ³B. E. Wyslouzil and G. Wilemski, *J. Chem. Phys.* **105**, 1090 (1996).
- ⁴A. L. Greer, P. V. Evans, R. G. Hamerton, D. K. Shangguan, and K. F. Kelton, *J. Cryst. Growth* **99**, 38 (1990).
- ⁵For large values of i and j the difference between the two entropies of mixing is of order $\ln(i+j)$ and is negligible with respect to the other terms which are of order i or j .
- ⁶G. Wilemski (unpublished).
- ⁷D. Stauffer, *J. Aerosol Sci.* **7**, 319 (1976).
- ⁸G. Wilemski, *J. Chem. Phys.* (to be published).
- ⁹J. S. Li and K. Nishioka, *Chem. Phys. Lett.* **295**, 211 (1998).
- ¹⁰J. S. Li, K. Nishioka, and I. L. Maksimov, *Phys. Rev. E* **58**, 7580 (1998).
- ¹¹References 9 and 10 contain the more general result that $r_s \tan \omega = J_B/J_A$ everywhere.
- ¹²R. McGraw, "Thermodynamic properties of multicomponent nuclei in vapor-liquid nucleation," presented at the 72 ACS Colloid and Surface Science Symposium, The Pennsylvania State University, June 21–24, 1998.
- ¹³H. Trinkaus, *Phys. Rev. B* **27**, 7372 (1983).
- ¹⁴I. S. Gradshteyn and I.M. Ryzhik, *Table of Integrals, Series, and Products* (Academic, New York, 1980), p. xxxii.
- ¹⁵P. G. Debenedetti and H. Reiss, *J. Chem. Phys.* **108**, 5498 (1998).
- ¹⁶G. Wilemski, *J. Chem. Phys.* **88**, 5134 (1988).
- ¹⁷P. Mirabel and J. L. Clavelin, *J. Aerosol Sci.* **9**, 219 (1978).
- ¹⁸"Well! I've often seen a cat without a grin," thought Alice; "but a grin without a cat! It's the most curious thing I ever saw in all my life!" Lewis Carroll, *Alice's Adventures in Wonderland* (Macmillan, London, 1865).